Korean J. Chem. Eng., 38(6), 1248-1259 (2021)
DOI: 10.1007/s11814-021-0784-6

pISSN: 0256-1115
eISSN: 1975-7220

Impact of g-C_3N_4 loading on NiCo LDH for adsorptive removal of anionic and cationic organic pollutants from aqueous solution

Harpreet Kaur, Satnam Singh, and Bonamali Pal†

School of Chemistry and Bio-Chemistry, Thapar Institute of Engineering and Technology, Patiala, 147004, India
(*Received 15 December 2020 • Revised 24 February 2021 • Accepted 13 March 2021*)

Abstract−Layered double hydroxides are traditional positively charged inorganic materials generally considered as efficient and low-cost adsorbents for the removal of anionic organic molecules. In this study, we prepared a series of g-C_3N_4@NiCo LDH composites by loading 10-30 wt% of g-C_3N_4 onto the LDH through the electrostatic self-assembly method. The bare LDH and g-C_3N_4 loaded LDH composites were characterized by XRD, SEM-EDS, Zeta, DLS, and FTIR techniques. Results revealed that extra peak corresponds to g-C_3N_4 originating in the XRD patterns, distorted morphology of LDH, reduction in positive surface zeta potential, and enhancement in hydrodynamic size after loading of g-C_3N_4 affirmed the successful formation of the composite. The adsorption performance of as-modified LDH was evaluated by removing the most commonly used salicylic acid and methylene blue as anionic and cationic model pollutant, respectively, from aqueous solution. The adsorption mechanism for both the pollutants by as-synthesized samples follows Langmuir isotherm. The results demonstrated that the bare LDH exhibited maximum adsorption efficiency of 75.16 mg/g and only 3.66 mg/g for salicylic acid and methylene blue, respectively. With 30 wt% loading of g-C_3N_4, the adsorption capacity for methylene blue increased to 25.16 mg/g almost 6-7 times higher than that of bare LDH. On the other hand, the opposite effect on adsorptive removal of salicylic acid was observed with increase in the wt% loading of g-C_3N_4. With 30 wt% loading of g-C_3N_4, the adsorption capacity for salicylic acid decreased to 38.37 mg/g, almost half that of bare LDH. A possible mechanism has been proposed. The kinetics for adsorption of salicylic acid onto bare LDH obeys the second-order model aside from the methylene blue adsorption which follows first-order kinetics. On the other hand, the kinetics of adsorption for both the pollutants onto (10-30) CN- LDH composites follows second order kinetics.

Keywords: g-C_3N_4@NiCo LDH Composite, Adsorptive Removal, Interactions Of Ionic Pollutants, Electro-kinetic Studies, Adsorption Isotherms, Surface Charge Variation

INTRODUCTION

Water contamination has become a most serious issue in the public arena causing several medical problems. One of the main reasons is the release of organic pollutants as effluents from industries into water sources [1-3]. To get rid of such kind of pollution, various techniques such as ion exchange [4], photocatalytic degradation [5], coagulation [6], adsorption [7], membrane separation [8] are used for water purification. Among them, adsorption is considered an easy, simple, economic, and highly effective method that is being extensively adopted worldwide to remove organic pollutants from water.

For the last few years, layered double hydroxides (LDH), mesoporous inorganic compounds commonly known as hydrotalcite or anionic clays are receiving incredible consideration in the adsorption research field. Their chemical composition is described as $[M^{2+}_{(1-x)}M^{3+}_{(x)}(OH)_2]^{x+}(A^{n-})_{x/n}\cdot mH_2O$, where M^{2+} and M^{3+} represents bivalent and trivalent metal ions, respectively, while A^{n-} are intercalated anions, and x is the stoichiometric ratio of $M^{3+}/(M^{2+}+M^{3+})$, having value within 0.2-0.33 range. They consist of positively charged hydroxide layers known as brucite layers and exchangeable anions in the interlayer region between two brucite layers [9-11]. Owing to low cost, high surface area, porous structure, non-toxicity, and excellent anion exchange capability, they are serving as efficient adsorbents capable of adsorbing toxic metal cations and anions, harmful organic dyes, herbicides, pesticides, toxic gases, pharmaceutical wastes, and various other pollution causing compounds [3,12,13]. Adsorption is a surface phenomenon that usually occurs due to certain kinds of intermolecular interactions between the adsorbate and adsorbent. Because of the positively charged surface, LDHs are highly effective adsorbents for the adsorption of harmful anionic organic compounds, whereas have low affinity towards cationic organic species due to ionic repulsions. Several modifications such as the intercalation of surfactants into their interlayer gallery [14], coupling with other adsorbing materials (graphene oxide [15], multiwalled carbon nanotubes [16], biochar [17], etc.) are being adapted to LDHs for improving their adsorption activity towards anionic as well as cationic organic compounds.

Recently, Zhang et al. fabricated NiFe LDH-montmorillonite composite consisting of the positively charged LDH nanoflakes on the negatively charged surface of montmorillonite. They investigated the adsorption performance of the composite towards both the anionic and cationic dye [18]. Li et al. modified the surface of MgAl LDH from hydrophilic to hydrophobic by intercalating organic surfactant for efficient removal of non-ionic, anionic, and cationic

†To whom correspondence should be addressed.
E-mail: bpal@thapar.edu

dyes [19]. However, utilization of cost-effective, easily synthesized, non-toxic materials as adsorbents is of high concern nowadays. Graphitic carbon nitride (g-C_3N_4), one of the most stable allotropes of carbon, is a non-toxic, easily synthesized, and environment-friendly compound having a high surface area. It consists of uniformly arranged tri-s-triazine (C_6N_7) units containing hydrophobic and π-π interactions, and can be used as an efficient adsorbent for various toxic metal cations and organic molecules. The surface of g-C_3N_4 is charged negatively due to the lone pair of electrons on nitrogen atoms present in tri-s-triazine units [20-22]. The formation of composite constituting LDH and g-C_3N_4 can come out as an effective adsorbent towards organic pollutants owing to their environment-friendly nature, non-toxicity, and synergic effect.

In this report, the positively charged NiCo LDH was coupled with negatively charged g-C_3N_4 and the effect of g-C_3N_4 loading onto the surface of LDH has been demonstrated for the adsorption of anionic and cationic pollutants. Salicylic acid having the chemical formula $C_7H_6O_3$ is an anionic organic compound generally utilized in dyestuff and pharmaceutical industries as a key ingredient in numerous skincare products. A large amount of salicylic acid as waste is generated due to poor separation of products causing various health issues like headaches, gastric irritation, and diarrhea, and can even bring about death if consumed in high concentrations [23,24]. On the other hand, methylene blue having the chemical formula $C_{16}H_{18}ClN_3S$ is a cationic organic compound broadly utilized in numerous industries such as pharmaceuticals, textiles, paper, and cosmetics. The waste dye discharged from industries into the environment can cause genuine health problems like hypertension, abdominal pain, bladder irritation, and nausea [25, 26]. Thus, these harmful pollution causing compounds need to be removed from the environment.

The main objective of the current report was to evaluate the adsorption performance of NiCo LDH itself and to investigate the effect of g-C_3N_4 loading on its adsorption behavior towards salicylic acid and methylene blue chosen as model pollutants. Parameters like adsorbent dosage, initial pollutant concentration, and contact time were optimized using bare LDH. The adsorption performance of bare LDH, different 10-30 wt% g-C_3N_4 loaded LDH composites were then analyzed and compared under optimum conditions. The Langmuir and Freundlich isotherm models were used to discuss the adsorption phenomenon. The kinetics of adsorption was demonstrated using the two most important first and second order kinetic models.

EXPERIMENTAL SECTION

1. Chemicals and Reagents

Cobalt nitrate hexahydrate ($Co(NO_3)_2{\cdot}6H_2O$), Nickel nitrate hexahydrate ($Ni(NO_3)_2{\cdot}6H_2O$), Ammonium Chloride (NH_4Cl), Sodium Hydroxide (NaOH), Melamine, Salicylic acid, and Methylene blue were purchased from Loba Chemie, India. Distilled water (D.I.) was obtained from Milli-Q, Millipore an ultrafiltration system.

2. Synthesis of NiCo LDH, g-C_3N_4 Nanosheets, and g-C_3N_4/NiCo LDH Composites

2-1. Synthesis of NiCo LDH

NiCo LDH was synthesized by the easy and simple co-precipitation method [27]. A metallic solution was prepared by dissolving 0.45 mmol of $Ni(NO_3)_2{\cdot}6H_2O$ and 0.30 mmol of $Co(NO_3)_2{\cdot}6H_2O$ in 20 ml of distilled water. Then, 4 mmol of NH_4Cl, and 2.06 mmol of NaOH were added simultaneously to the above prepared metallic solution and magnetically stirred at 600 rpm for about 30 min. The mixture was transferred to an oven and aged at 55 °C for 15 h. After cooling to room temperature, the obtained precipitates were collected by centrifuging the solution at 6,000 rpm for 5 min, washed with distilled water several times followed by ethanol. The sample was then dried for 12 h at 60 °C. The as-prepared NiCo LDH sample is abbreviated as bare LDH.

2-2. Synthesis of g-C_3N_4 Nanosheet

First, bulk graphitic nitride powder was prepared by placing about 5 g of melamine in a silica crucible, covered, and heated in a muffle furnace at 550 °C for 4 h with a heating rate of 5 °C/min. The bulk g-C_3N_4 yellow powder was collected until it cooled to room temperature and was crushed into a fine powder using a mortar pestle.

To prepare the g-C_3N_4 nanosheet, the obtained bulk g-C_3N_4 yellow powder was further calcined for another 2 h at 530 °C with a heating rate of 5 °C/min. The obtained pale yellow product was g-C_3N_4 nanosheet powder [28,29]. The prepared g-C_3N_4 nanosheet is abbreviated as CN.

2-3. Preparation of g-C_3N_4 Loaded NiCo LDH Composites

The g-C_3N_4@NiCo LDH composites with different weight percentages of g-C_3N_4 were prepared by the electrostatic assembly method. An appropriate amount of g-C_3N_4 powder was added into a beaker containing water and sonicated for 60 minutes to completely disperse the g-C_3N_4 particles. The LDH powder was taken in another water containing beaker and sonicated for 60 minutes. After the complete dispersion, both the solutions were mixed together and magnetically stirred at 600 rpm for about 24 hours [30]. The different 10, 20, and 30 wt% g-C_3N_4@LDH composites are abbreviated as 10CN-LDH, 20CN-LDH, and 30CN-LDH, respectively.

3. Adsorbent Characterization

The XRD patterns were studied using X-ray diffractometry (XRD, Xpert pro) using Cu-Kα (1.54 Å) operating at 45 kV with diffraction angle 2θ (10^o to 80^o). Scanning electron microscopy and energy dispersive microscopy (SEM-EDS, JEOL JSM-7600 F, 01 operating at 30 kV) were used for morphological study and elemental composition analysis. The zeta potential value of synthesized samples was evaluated using a Zeta analyzer (ZEN 3600, Malvern, U.K.) and their hydrodynamic size was analyzed using the dynamic light scattering technique (DLS). For this purpose, about 2 mg of prepared adsorbent was dispersed in 10 ml of distilled after sonicating for about 30 min. The FTIR spectra of samples were recorded using an Agilent FTIR spectrophotometer. The concentration of a pollutant in the solution was determined by a Shimadzu UV-2600 spectrophotometer.

4. Adsorption Activity

The adsorption behavior of adsorbents (bare LDH and different (10-30) CN-LDH composites) was observed using a 30 ml solution of pollutants. The effect of various parameters such as the concentration of pollutants (5-55 mg/L for salicylic acid and 2-50 mg/L for methylene blue), amount of adsorbent (2-20 mg), and contact

time (2-30 min for salicylic acid and 15-210 min for methylene blue) was investigated. A set of beakers, each beaker containing 30 ml of pollutant solution of a particular concentration and the appropriate amount of adsorbent, was prepared and stirred at 600 rpm using a magnetic stirrer under dark for different time intervals. After stirring for a fixed time, each beaker was removed, 5 ml of its aqueous sample was taken and centrifuged to separate the adsorbent. The concentration of adsorbate in the supernatant was measured using a UV-Visible spectrophotometer at maximum absorbance (λ_{max}=296 and 664 nm for salicylic acid and methylene blue, respectively). The adsorption capacity (adsorbed mass per unit mass, mg/g) of the adsorbents was calculated using the following equation:

$$Q_e=(C_o-C_e)\frac{V}{W} \quad (1)$$

where C_o signifies the initial concentration of pollutant (mg/L), C_e is the concentration of the pollutant in the solution at equilibrium (mg/L), V is the volume of solution (L), W is the amount of adsorbent (g), and Q_e is the adsorption efficiency of the adsorbent (mg/g) at equilibrium. The percentage (R%) of salicylic acid and methylene blue adsorbed onto adsorbents was calculated using the following equation:

$$R\%=\frac{(C_o-C_e)}{C_o}\times 100 \quad (2)$$

where R% is the pollutant adsorbed (%), C_o and C_e is the initial and equilibrium concentration of pollutant in the solution, respectively [47,48].

RESULTS AND DISCUSSION

1. Characterization

The XRD spectra of bare NiCo LDH, g-C_3N_4, and 10CN-LDH, 20CN-LDH, 30CN-LDH composites were studied. Fig. 1 shows the XRD pattern of prepared samples. The peaks observed at 2θ value of 11.0°, 22.2°, 34.1°, and 60.6° correspond to (003), (006), (009), and (110) planes, respectively, of a regular LDH material (JCPDS No. 38-0486) [27,31]. The peak at 2θ value of 27.5° was indexed to pure g-C_3N_4 [20]. In the case of CN-LDH composites, all the peaks of pure LDH are present along with an additional peak originating at 2θ=27.5° corresponding to g-C_3N_4 confirming its presence in composites. This peak intensity increases with an increase in the wt% loading (10-30) of g-C_3N_4 in the LDH sample demonstrates the successful formation of the composite. More-

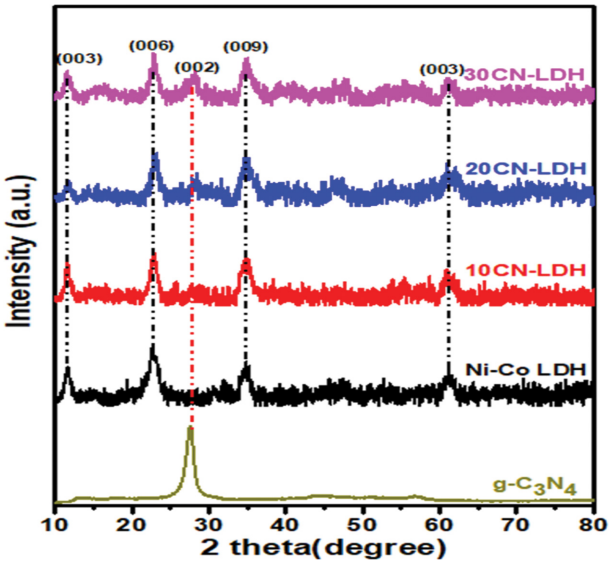

Fig. 1. X-ray diffraction patterns of g-C_3N_4, NiCo LDH, and different 10, 20, and 30 CN-LDH composites.

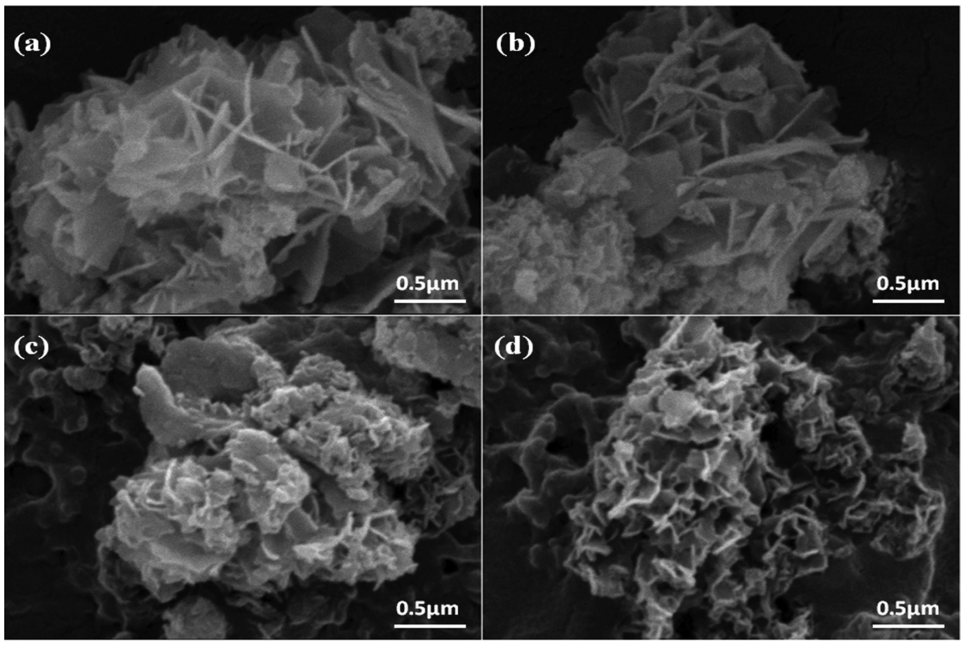

Fig. 2. SEM images of NiCo LDH ((a) and (b)) and 30CN-LDH composite ((c) and (d)).

over, after being modified with g-C_3N_4, no significant change was observed in diffraction peak intensity and peak position of pure LDH, confirming the preservation of its crystal structure phase.

SEM analysis was performed to examine the surface morphology of bare LDH and CN-LDH composites. The SEM image (Fig. 2) of bare LDH shows the petal-like morphology comprised of sharp petals oriented and interconnected in certain directions. Such morphology provides more contact area and space for the reaction to take place on the surface [27,32]. On the other hand, in the case of the 30CN-LDH composite, a significant change in morphology than bare LDH is observed. The sharp petals are missing and the petal-like surface morphology gets distorted, which can be due to the stacking of negatively charged g-C_3N_4 nanosheets on the positively charged surface of LDH.

The elemental dot mapping and EDS spectra for the 30CN-LDH composite representing the atomic and weight percentage of elements are shown in Fig. 3. The elemental mapping confirms the presence of Ni, Co, O, Cl, C, and N elements appearing in purple, blue, green, sky-blue, red, and yellow regions, respectively. Similarly, EDS spectra confirm their elemental composition. The wt%

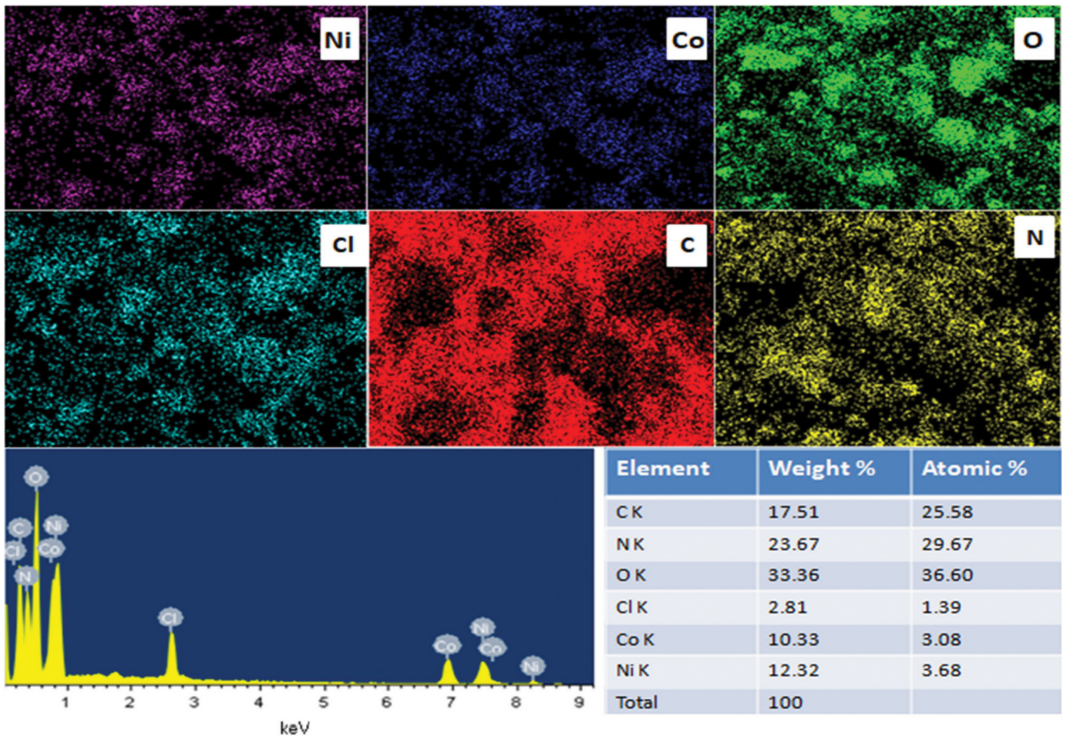

Element	Weight %	Atomic %
C K	17.51	25.58
N K	23.67	29.67
O K	33.36	36.60
Cl K	2.81	1.39
Co K	10.33	3.08
Ni K	12.32	3.68
Total	100	

Fig. 3. Elemental dot mapping and EDS spectra of 30CN-LDH composite showing elemental composition.

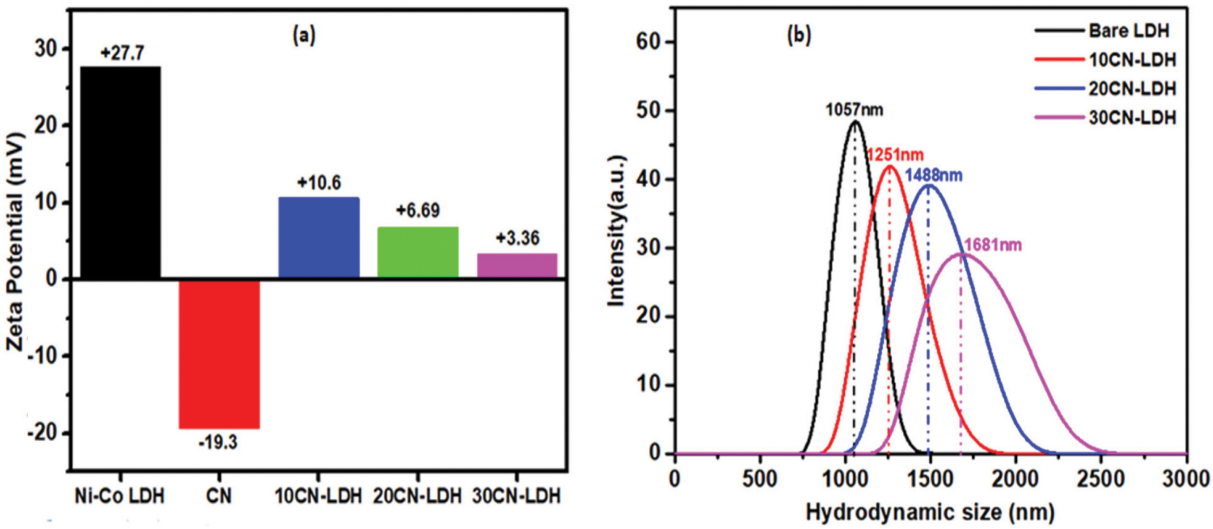

Fig. 4. Zeta potential variation (a), and hydrodynamic particle size (b) of NiCo LDH, CN, and different 10, 20, and 30 CN-LDH composites.

distribution of elements is as 17.51, 23.67, 33.36, 2.81, 10.33, and 12.32% for C, N, O, Cl, Co, and Ni, respectively.

The electrokinetic studies of as-synthesized samples were examined using zeta and DLS analysis. As shown in Fig. 4(a), the zeta potential of bare LDH is observed at +27.7 mV due to the positive charge of brucite layers that arises through partial substitution of Ni^{2+} by Co^{3+} ions in the formation of double hydroxide layers. The zeta potential value of pure g-C_3N_4 is to be −19.3 mV due to the presence of tri-s-triazine units containing nitrogen pots having a lone-pair of electrons responsible for its negatively charged surface. For composites, the zeta potential value is observed at +10.6, +6.69, and +3.36 mV for 10, 20, and 30CN-LDH composite. The decrease in the zeta potential with an increase in the wt% loading of g-C_3N_4 is due to electrostatic interactions between the positively charged LDH and the negatively charged g-C_3N_4 that neutralize the positive charge on the LDH surface [30].

As per the dynamic light scattering technique, a variation in hydrodynamic particle size of LDH is observed with variable wt% stacking of g-C_3N_4 (Fig. 4(b)). The particle size of bare LDH is 1,057 nm, which increases to 1,251, 1,488, and 1,681 nm in the case of 10, 20, and 30CN-LDH composites, respectively. The expansion in the particle size of CN-LDH composites can be due to the deposition of g-C_3N_4 nanosheets onto the surface of LDH.

The FTIR spectra of bare LDH and 30CN-LDH composite are shown in Fig. 5. The spectra of LDH reveal the presence of hydroxyl groups, intercalated anions, and metal ions in the brucite layers. A broad absorption band positioned at about 3,400 cm^{-1} is the O-H stretching band that corresponds to the metal hydroxyl groups and interlayer water molecules. The band at 1,622 cm^{-1} is due to the bending vibration of water molecules. The band at 1,350 cm^{-1} emerges due to the presence of intercalated nitrate anions [33,34]. The bands in the low-frequency region 500-900 cm^{-1} corresponds to metal-oxygen (Ni-O and Co-O) and metal-oxo-bridge linkage (Ni-O-Co) bands [30,35]. In the case of the 30CN-LDH composite, the additional peak originating at about 3,500 cm^{-1} can be ascribed to the stretching vibration modes of uncondensed N-H groups of g-C_3N_4 [29]. The presence of g-C_3N_4 can be credited to the sharpness of bands appearing in the region 1,350 to 1,650 cm^{-1} due to vibration modes of sp^2 C-N stretching and out-of-plane bending vibrations of sp^3 C-N bonds. The peak originating at 834 cm^{-1} corresponds to the out-of-plane bending vibration of s- triazine units

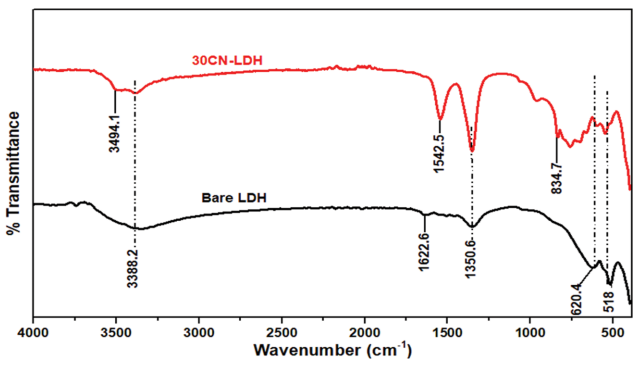

Fig. 5. The FTIR spectrum of as prepared bare LDH and 30CN-LDH composite.

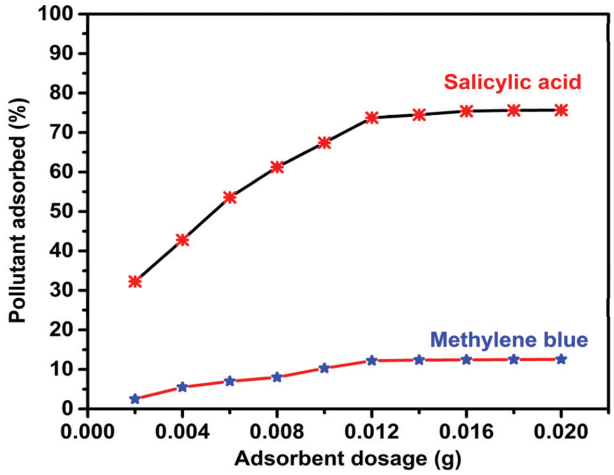

Fig. 6. Effect of dosage of bare LDH on salicylic acid and methylene blue removal from the aqeous solution. Salicylic acid concentration- 40 mg/L, and methylene blue concentration-10 mg/L.

[20,36]. Moreover, after the addition of g-C_3N_4, the bands representing the pure LDH phase in CN-LDH composite spectra show little shift from that in bare LDH spectra. These results indicate the effect and presence of g-C_3N_4 on LDH through interfacial electrostatic interaction [29].

2. Adsorption Studies

2-1. Parameter Optimization

2-1-1. Effect of Adsorbent Dosage

The adsorption process of adsorbate on the surface of the adsorbent varies directly with its dosage. It is because the number of adsorption sites increases with the increase in the dose of adsorbent until saturation [37]. The effect of the dosage of bare LDH towards the adsorption of negatively charged salicylic acid and positively charged methylene blue is represented in Fig. 6. According to the observation, 0.012 g of LDH removes about 73.8% of salicylic acid. No significant change in adsorption efficiency of LDH was observed with further increasing its dosage due to reaching saturation. On the other hand, 0.012 g of LDH dosage exhibits the maximum of only 12.5% removal of methylene blue dye showing saturation with more amount of LDH dosage. Here, no rise in adsorption efficiency is found by further increasing the concentration of LDH, which indicates the saturation of active sites. Therefore, 0.012 g of LDH dosage is optimized for the adsorption of both the pollutants.

2-1-2. Effect of Initial Concentration of Adsorbate

The effect of initial concentration of pollutants on the adsorption efficiency of LDH was investigated by varying the concentration of salicylic acid and methylene blue in the range 5-55 mg/L and 2-50 mg/L, respectively. As illustrated in Fig. 7, the highest adsorption efficiency of 73.7 mg/g is observed at 35 mg/L initial concentration of salicylic acid and a plateau at higher concentrations representing the saturation of adsorption sites [38,39]. On the other hand, for methylene blue, the adsorption efficiency is a maximum 3.03 mg/g at 10 mg/L of its initial concentration. It then decreases with further increasing the initial concentration of methylene blue and even becomes zero at higher concentrations show-

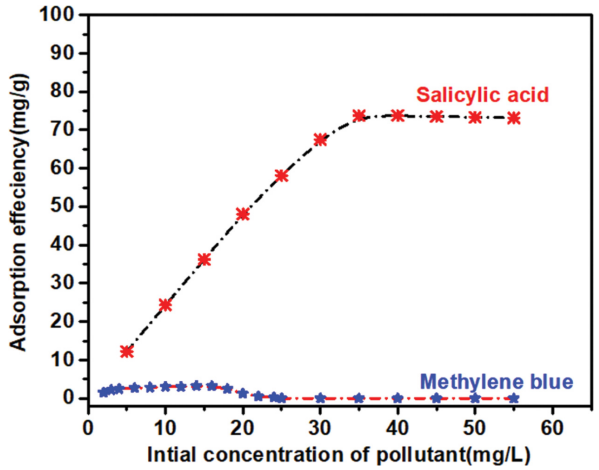

Fig. 7. Effect of pollutant concentration on adsorption efficiency by bare LDH. Adsorbent dosage- 0.012 g, salicylic acid concentration (5-55 mg/L), methylene blue concentration (2-55 mg/L).

ing no adsorption.

2-1-3. Effect of Contact Time

The contact time between adsorbate and adsorbent plays a crucial role in the adsorption process, as the adsorption increases with an increase in contact time until reaching equilibrium [37,39]. As shown in Fig. 8(a), more than 60% of salicylic acid was rapidly adsorbed in first 2 min on the surface of bare LDH and then adsorbed slowly with time. The maximum adsorption of about 84% of salicylic occurred within only 20 min with no further increment as equilibrium was achieved. For methylene blue (Fig. 8(b)), equilibrium was achieved in 150 min with only 12.5% of dye adsorbed. The adsorption of salicylic acid was efficiently high on the surface of LDH. It can be due to its petal-like morphology that provides a large contact area and electrostatic interactions between its surface and salicylic acid molecules. On the other hand, the ionic repulsion between the positively charge brucite layers of LDH and methylene dye molecules was responsible for the lesser adsorption of methylene blue.

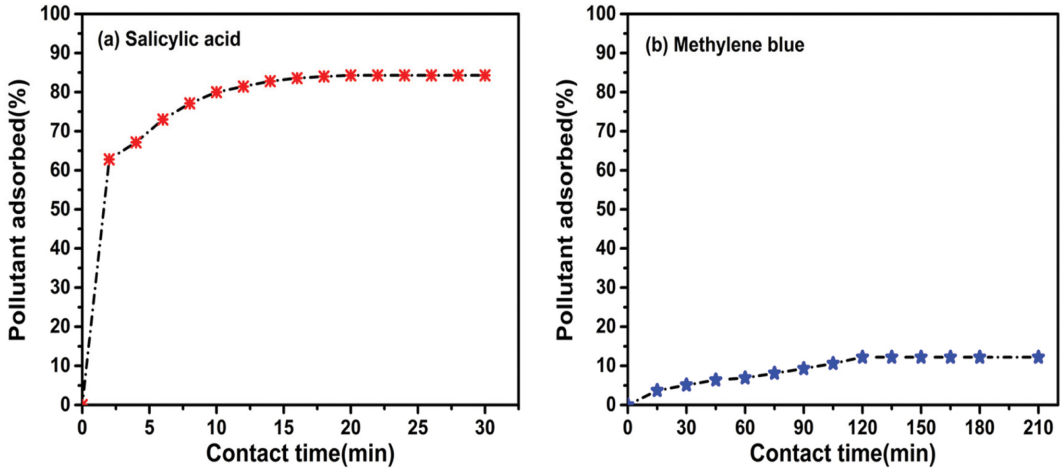

Fig. 8. Effect of contact time on adsorption behavior of bare LDH towards salicylic acid and methylene blue. Adsorbent dosage- 0.012 g, Salicylic acid concentration- 35 mg/L, methylene blue concentration-10 mg/L.

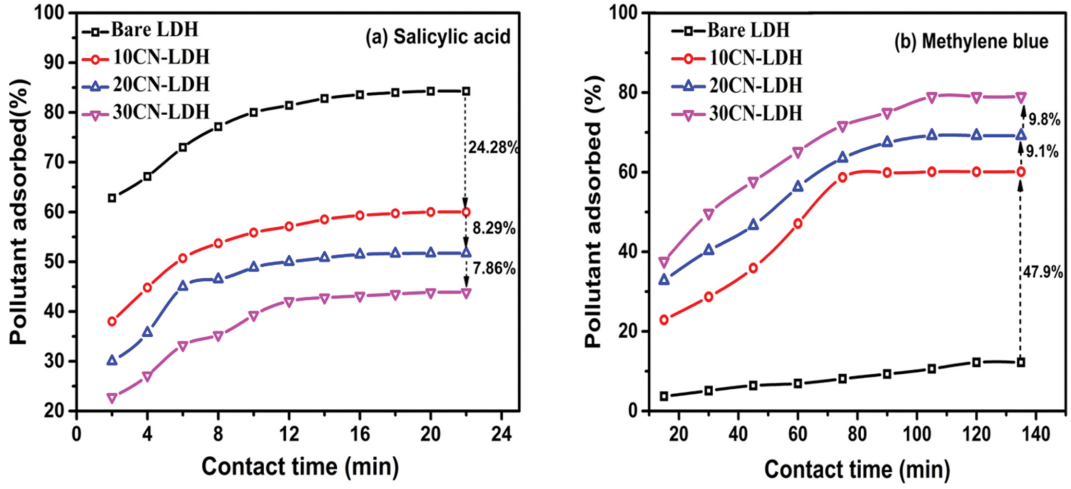

Fig. 9. Influence of g-C_3N_4 loading on adsorption behavior of bare LDH, (a) for salicylic acid, (b) for methylene blue. Adsorbent dosage- 0.012 g, Salicylic acid concentration- 35 mg/L, methylene blue concentration-10 mg/L.

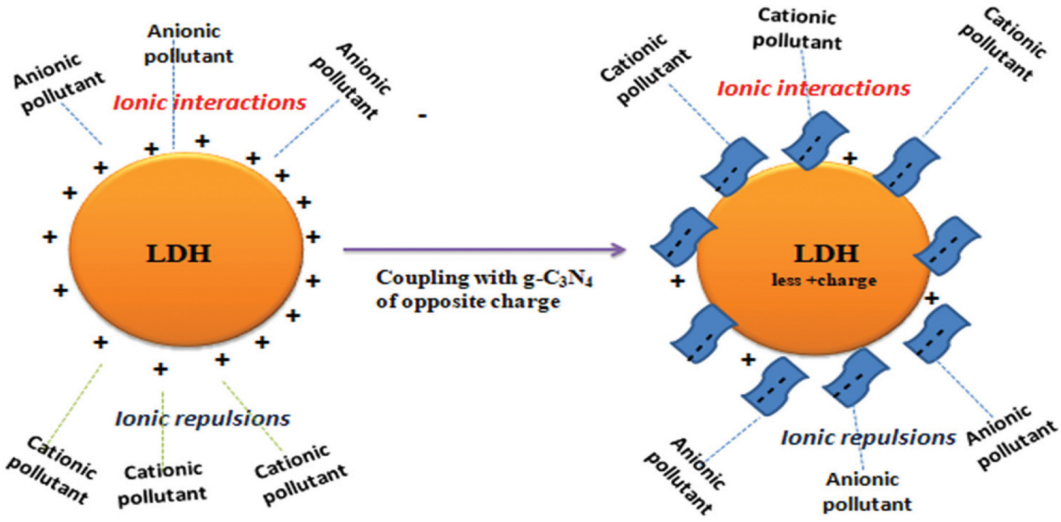

Scheme 1. A schematic representation of surface modification of LDH with loading of g-C_3N_4 and adsorption mechanism of cationic and anionic pollutants.

2-2. Influence of g-C_3N_4 Loading

As represented in Scheme 1, the loading of negatively charged g-C_3N_4 onto the surface of LDH brought an adverse change in its adsorption behavior by decreasing its surface positive charge. The decrease in surface positive charge of LDH with loading of g-C_3N_4 onto its surface improved its adsorption efficiency towards methylene blue, whereas showing an exactly opposite behavior for salicylic acid. As shown in Fig. 9, with an increase in the wt% loading of g-C_3N_4 on LDH, the adsorption efficiency of LDH decreases towards salicylic acid but increases towards methylene blue. The 30CN-LDH composite with the highest 30 wt% g-C_3N_4 loading exhibiting maximum adsorption efficiency of 79% for methylene blue is almost 6-7 times higher than bare LDH. It can be due to the presence of negatively charged g-C_3N_4 nanosheets onto the surface of LDH that results in a decrease in its surface charge and provides adsorption sites for methylene blue. For salicylic acid, in the case of 30CN-LDH composite, the adsorption efficiency decrease to 43.75% is about two times less than bare LDH.

2-3. Adsorption Isotherms

To confirm the adsorption phenomenon, the 30 ml of solutions of salicylic acid and methylene blue with an initial concentration of 35 mg/L and 10 mg/L, respectively, were stirred in the presence of 0.012 g of adsorbent under dark for 12 hours. As shown in Fig. S1 and Fig. S2, no significant change in the absorbance value was observed with 12 hours of contact time than 20 and 150 min for salicylic acid, methylene blue, respectively. It affirmed that the adsorption of pollutants takes place on the surface of the adsorbent. Fig. S3(a), (b) shows the graph between C_e vs Q_e representing the adsorption of salicylic acid and methylene blue over bare LDH and (10-30) CN-LDH composites. The adsorption capacity increased initially with an increase in the equilibrium concentration and then reached a plateau due to saturation of active sites.

The adsorption process of adsorbate at equilibrium was described using the two most common adsorption isotherm models: Langmuir and Freundlich. The adsorption isotherms were investigated by changing the initial concentration of pollutants (5-55 mg/L for salicylic acid and 2-10 mg/L for methylene blue) added to a certain amount (0.012 g) of the adsorbent. Langmuir isotherm is based on the homogeneous adsorption through the formation of a monolayer of adsorbate on the surface of the adsorbent with identical adsorption sites having equivalent energy. It is also assumed that there are no interactions between the adjacent adsorbed molecules as one molecule adsorbs on one adsorption site. The Langmuir adsorption isotherm is expressed as follows:

$$Q_e = \frac{Q_{max} K_L C_e}{1 + K_L C_e} \tag{3}$$

The linear form of the Langmuir isotherm equation is as follows:

$$\frac{C_e}{Q_e} = \frac{1}{Q_{max} K_L} + \frac{C_e}{Q_{max}} \tag{4}$$

where k_L (L/mg) is Langmuir constant representing affinity of adsorbate towards adsorbent, C_e (mg/L) is the concentration of adsorbate at equilibrium, Q_e (mg/g) is the adsorption capacity of adsorbent at equilibrium, Q_{max} (mg/g) is the maximum adsorption capacity of adsorbent up to complete monolayer formation. The graph was plotted between C_e/Q_e vs C_e (Fig. 10) and the intercept and slope obtained from the graph were used to calculate k_L and Q_{max} values. The nature of adsorption whether the process is favorable or unfavorable can be concluded through a dimensionless constant, R_L expressed as:

$$R_L = \frac{1}{1 + K_L C_o} \tag{5}$$

where k_L is the Langmuir constant, C_o is the highest initial concentration of pollutant. The value of R_L suggests the adsorption nature, R_L=0 (irreversible), 0<R_L<1 (favorable), R_L=1 (linear), or R_L>1 (non-favorable) [40].

The Freundlich isotherm is based on the assumption that the surface of the adsorbent is heterogeneous and there exist strong

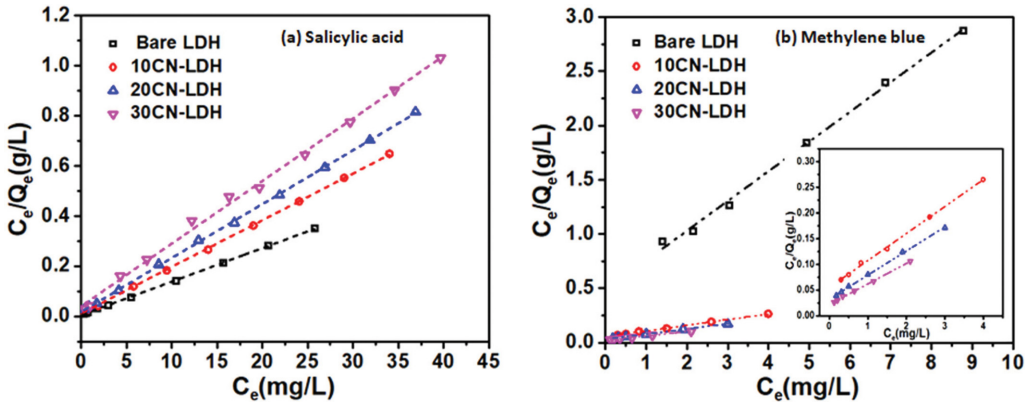

Fig. 10. Modeling of adsorption equilibria by Langmuir isotherm. (a) salicylic acid and (b) methylene blue by NiCo LDH and (10-30) CN-LDH composites.

interactions between the adsorbate molecules. The adsorption takes place on the surface of the adsorbent through the multilayer formation of the adsorbate molecules. The equation of the Freundlich isotherm is represented as follows:

$$Q_e = k_F C_e^{1/n} \quad (6)$$

The linear form of Freundlich model is described by the following equation:

$$\log Q_e = \frac{1}{n} \times \log C_e + \log k_F \quad (7)$$

where k_F is the Freundlich constant, 1/n is the heterogeneity factor that describes the favorability of adsorption, Q_e (mg/g) is the amount of pollutant adsorbed at equilibrium, C_e (mg/L) is the concentration of the pollutant in solution at equilibrium. The values of n greater than unity indicate the process to be favorable [41,42]. The plot of $\log Q_e$ vs $\log C_e$ for both pollutants is shown in Fig. 11. Both the Langmuir and Freundlich models fitted the experimental data. Their corresponding parameters calculated from the slope and intercept of their respective graphs are mentioned in Table 1. According to the results displayed, the value of R^2 (correlation coefficient) for Langmuir model was found in the range 0.9957-0.9996, higher and closer to unity than the R^2 values for the Freundlich model in the range 0.7987-0.9694 for bare LDH and CN-LDH composites. Therefore, a better fit was observed for Langmuir than the Freundlich model, which suggests the adsorption of pollutants through monolayer formation at the surface of adsorbents. Also, the adsorption capacity calculated using the Langmuir model equation was found closer to that obtained from experimental data. Hence, the adsorption of pollutants follows the Langmuir model and takes place at a homogeneous surface of the adsorbent where each pollutant molecule is fairly distributed on its surface. Moreover, the calculated R_L values using the Langmuir model equation lie in the range of 0-1, indicating the favorable adsorption of both the pollutants. The favorability of adsorption can also be deduced from the Freundlich parameter, n, which was found more than unity (1.936-3.941).

2-4. Kinetic Study

The kinetics of adsorption of salicylic acid and methylene blue over bare LDH and CN-LDH composites were studied to analyze their adsorption performance. To find their adsorption kinetics, pseudo-first-order and pseudo-second-order models were studied.

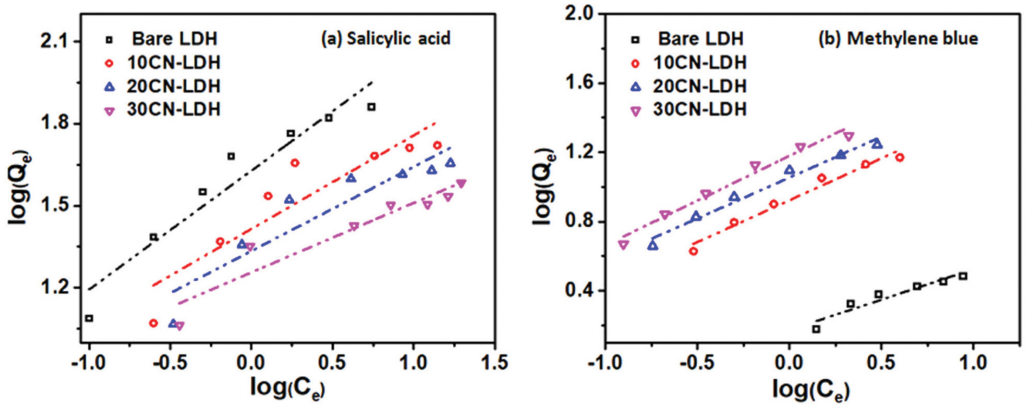

Fig. 11. Modeling of adsorption equilibria by Freundlich isotherm. (a) salicylic acid and (b) methylene blue by NiCo LDH and (10-30) CN-LDH composites.

The equation for pseudo-first-order model in linear form is expressed as follows:

$$\log(Q_e - Q_t) = \log Q_e - \frac{k_1}{2.303}t \quad (8)$$

Table 1. The calculated parameters of Langmuir and Freundlich models for adsorption of salicylic acid over bare LDH and CN-LDH composites are as follows

(a) Salicylic acid

	Langmuir model				Freundlich model		
Adsorbent	Q_{max}	K_L	R^2	R_L	K_F	n	R^2
Bare LDH	75.18	2.56	0.9996	0.007	42.4	2.305	0.9094
10CN-LDH	53.76	1.63	0.9996	0.011	26.0	2.929	0.7987
20CN-LDH	46.50	1.20	0.9996	0.149	21.6	3.254	0.8221
30CN-LDH	40.08	0.613	0.9996	0.028	18.0	3.941	0.8803

(b) Methylene blue

	Langmuir model				Freundlich model		
Adsorbent	Q_{max}	K_L	R^2	R_L	K_F	n	R^2
Bare LDH	3.66	0.566	0.9957	0.150	1.48	2.845	0.8924
10CN-LDH	19.02	3.827	0.9981	0.025	8.37	2.069	0.9648
20CN-LDH	21.34	1.444	0.9984	0.064	11.33	2.118	0.9694
30CN-LDH	25.07	1.819	0.9984	0.052	15.12	1.936	0.9688

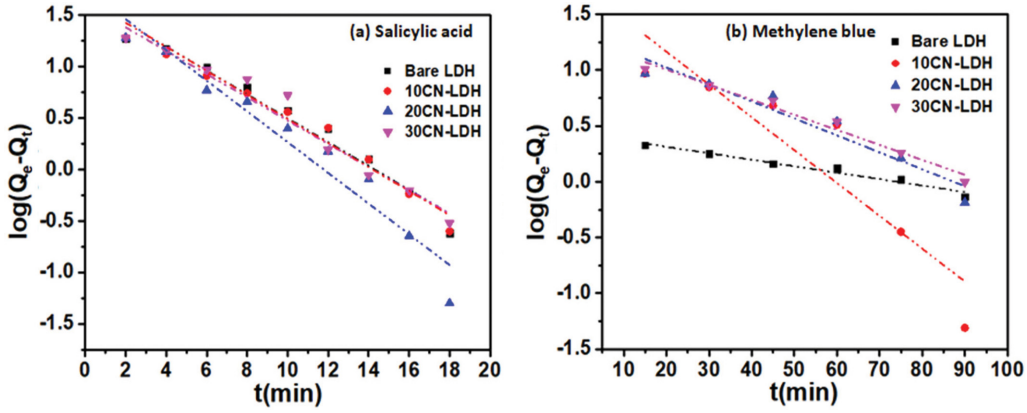

Fig. 12. Kinetics of adsorption of (a) salicylic acid and (b) methylene blue by NiCo LDH and (10-30) CN-LDH composites according to first order model.

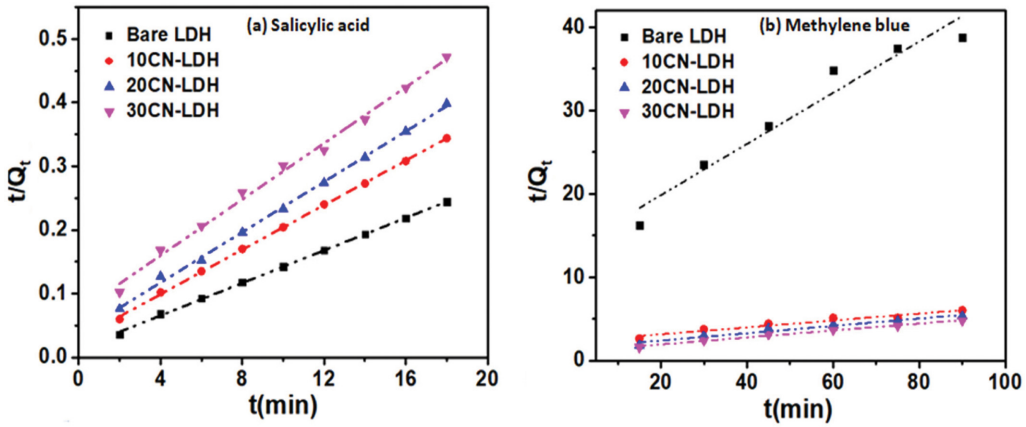

Fig. 13. Kinetics of adsorption of (a) salicylic acid and (b) methylene blue by NiCo LDH and (10-30) CN-LDH composites according to second order model.

where, Q_t and Q_e are termed as adsorption efficiencies (mg/g) at time t (min) and equilibrium, respectively, k_1 is the first-order rate constant (min^{-1}) [43,44]. The plots of $\log(Q_e - Q_t)$ vs t for both the pollutants salicylic acid and methylene blue are shown in Fig. 12(a) and (b).

The equation for pseudo-second-order model in linear form is expressed as follows:

$$\frac{t}{Q_t} = \frac{1}{k_2 Q_e^2} + \frac{t}{Q_e} \quad (9)$$

where, k_2 is the second-order rate constant, Q_t and Q_e represent the amount of adsorbate adsorbed per unit mass of the adsorbent (mg/g) at time t (min) and equilibrium, respectively [45,46]. The second-order kinetic model is based on the assumption that the rate-limiting step is chemisorption that involves share or exchange of electrons between the adsorbate and adsorbent. The plots of t/Q_t vs t for both the pollutants are shown in Fig. 13(a) and (b). The slope and intercept obtained from the graphs were used to calculate the parameters of first- and second-order kinetics as mentioned in Table 2. For salicylic acid, the R^2 values of the second-order model were found higher and closer to unity than that for first-order kinetics. It indicates that the adsorption of salicylic acid onto bare LDH and CN-LDH composites follows second-order kinetics. On the other hand, in the case of methylene blue, the R^2 values of the second-order model were closer to unity than that of the first-order model for CN-LDH composites except for bare LDH. The R^2 value of the second-order model was lower than that of the first-order model for bare LDH. The adsorption of methylene blue at the surface of bare LDH followed the first-order kinetics, whereas followed second-order kinetics at the surface of CN-LDH composites.

MECHANISTIC UNDERSTANDING

The NiCo LDH shows efficient adsorption towards salicylic acid, an anionic pollutant. It can be due to the electrostatic interaction between the negatively charged salicylic acid molecules and the

Table 2. The calculated parameters of first order kinetics and second order kinetics for the adsorption of (a) salicylic acid and (b) methylene blue over bare LDH and CN-LDH composites are as follows

(a) Salicylic acid

	First order kinetics			Second order kinetics		
Adsorbent	Q_e	k_1	R^2	Q_e	k_2	R^2
Bare LDH	45.19	0.266	0.9682	78.30	0.011	0.9995
10CN-LDH	40.24	0.260	0.9708	57.10	0.010	0.9995
20CN-LDH	57.05	0.343	0.9380	50.55	0.010	0.9982
30CN-LDH	45.45	0.268	0.9607	13.9	0.235	0.9936

(b) Methylene blue

	First order kinetics			Second order kinetics		
Adsorbent	Q_e	k_1	R^2	Q_e	k_2	R^2
Bare LDH	2.67	0.013	0.9587	3.25	0.006	0.9384
10CN-LDH	56.65	0.067	0.8055	24.18	0.007	0.9370
20CN-LDH	21.22	0.035	0.9109	22.66	0.001	0.9507
30CN-LDH	18.75	0.031	0.9713	24.0	0.001	0.9903

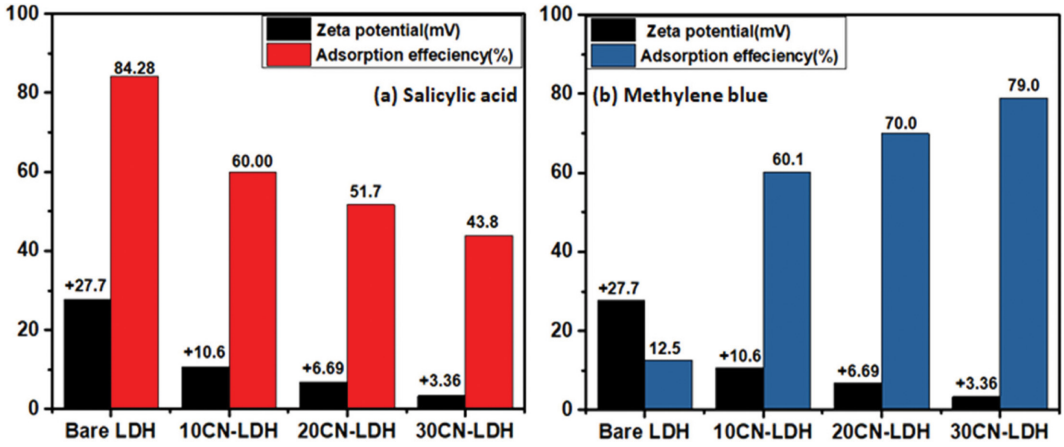

Fig. 14. Comparison of adsorption efficiency (%) of (a) salicylic acid and (b) methylene blue by variation of zeta potential of NiCo LDH and (10-30) CN-LDH composites.

positively charged surface of LDH. To confirm the adsorption phenomenon, the zeta potential values of adsorbents after the adsorption of pollutants were analyzed (Table S1). The zeta potential value of bare LDH after the adsorption of salicylic acid changed from +27.7 to −0.41 mV, suggesting the adsorption of salicylic acid on the surface of LDH through electrostatic interactions. Similarly, the zeta potential value for CN-LDH composites becomes more negative after the adsorption of salicylic acid. It may be due to the neutralization of the positive surface charge of LDH by adsorbed salicylic acid molecules and the presence of negatively charged g-C_3N_4. On the other hand, in the case of methylene blue, the surface zeta potential of bare LDH after contact with methylene blue increased from +27.7 to +29.7 mV. It can be due to the presence of adsorbed methylene blue molecules on the surface of LDH. Similarly, the zeta potential value of CN-LDH composites becomes more positive after the adsorption of methylene blue. It could be due to electrostatic interactions of methylene blue molecules with nitrogen atoms and π-π interactions with sp^2 hybridized carbon atom of g-C_3N_4 loaded on the surface of LDH [56,57]. The comparison study regarding the removal of pollutants depending upon the surface zeta potential of adsorbent is shown in Fig. 14.

CONCLUSION

This study explored that bare LDH having a positively charged surface was an efficient adsorbent for anionic pollutants but showed poor affinity towards cationic pollutants. After loading of g-C_3N_4, the adsorption behavior of LDH towards cationic pollutants improved as the coupling of LDH with negatively charged g-C_3N_4 nanosheets resulted in neutralizing its surface positive charge. Accordingly, by varying the content of g-C_3N_4 on LDH, the surface charge of the composite can be adjusted as desired to effectively remove the cationic and anionic pollutants from the aqueous solution. Hence, the formation of such hybrid materials can be a very beneficial strategy to design non-toxic, environment friendly, low cost, easily synthesized materials for wastewater treatment.

DECLARATION OF COMPETING INTEREST

The authors do not have any conflict of interest in the publication of the manuscript.

ACKNOWLEDGEMENT

The authors thank SAI labs, Thapar institute of engineering and technology for XRD, SEM-EDS analysis.

SUPPORTING INFORMATION

Additional information as noted in the text. This information is available via the Internet at http://www.springer.com/chemistry/journal/11814.

REFERENCES

1. D. E. Helbling, *Curr. Opin. Biotechnol.*, **33**, 142 (2015).
2. M. B. Ahmed, J. L. Zhou, H. H. Ngo and W. Guo, *Sci. Total Environ.*, **532**, 112 (2015).
3. M. Zubair, M. Daud, G. McKay, F. Shehzad and M. A. Al-Harthi, *Appl. Clay Sci.*, **143**, 279 (2017).
4. I. Levchuk, J. J. R. Márquez and M. Sillanpää, *Chemosphere*, **192**, 90 (2018).
5. N. Baliarsingh, K. M. Parida and G. C. Pradhan, *Ind. Eng. Chem. Res.*, **53**, 3834 (2014).
6. A. Talaiekhozani, M. R. Talaei and S. Rezania, *J. Environ. Chem. Eng.*, **5**, 1828 (2017).
7. R.-r. Shan, L.-g. Yan, Y.-m. Yang, K. Yang, S.-j. Yu, H.-q. Yu, B.-c. Zhu and B. Du, *J. Ind. Eng. Chem.*, **21**, 561 (2015).
8. C. Fonseca Couto, L. C. Lange and M. C. Santos Amaral, *J. Water Process Eng.*, **26**, 156 (2018).
9. L. Mohapatra, K. Parida and M. Satpathy, *J. Phys. Chem. C.*, **116**, 7350 (2012).
10. G. Zhang, X. Zhang, Y. Meng, G. Pan, Z. Ni and S. Xia, *Chem. Eng. J.*, **392**, 123684 (2020).
11. G. Arrabito, A. Bonasera, G. Prestopino, A. Orsini, A. Mattoccia, E. Martinelli, B. Pignataro and P. G. Medaglia, *Crystals*, **9**, 361 (2019).
12. A. Baruah, S. Mondal, L. Sahoo and U. K. Gautam, *J. Solid State Chem.*, **280**, 120963 (2019).
13. M. Zubair, N. Jarrah, M. S. Manzar, M. Al-Harthi, M. Daud, N. D. Mu'azu and S. A. Haladu, *J. Mol. Liq.*, **230**, 344 (2017).
14. P. Chakraborty and R. Nagarajan, *Appl. Clay Sci.*, **118**, 308 (2015).
15. Y. Zheng, B. Cheng, W. You, J. Yu and W. Ho, *J. Hazard. Mater.*, **369**, 214 (2019).
16. Y.-l. Long, J.-g. Yu, F.-p. Jiao and W. j. Yang, *Trans. Nonferrous Met. Soc. China English Ed.*, **26**, 2701 (2016).
17. D. Huang, C. Liu, C. Zhang, R. Deng, R. Wang, W. Xue, H. Luo, G. Zeng, Q. Zhang and X. Guo, *Bioresour. Technol.*, **276**, 127 (2019).
18. D. Bin Jiang, C. Jing, Y. Yuan, L. Feng, X. Liu, F. Dong, B. Dong and Y. X. Zhang, *J. Colloid Interface Sci.*, **540**, 398 (2019).
19. B. Zhang, Z. Dong, D. Sun, T. Wu and Y. Li, *J. Ind. Eng. Chem.*, **49**, 208 (2017).
20. Y. Yang, B. Mao, G. Gong, D. Li, Y. Liu, W. Cao, L. Xing, J. Zeng, W. Shi and S. Yuan, *Int. J. Hydrogen Energy*, **44**, 15882 (2019).
21. B. Ou, J. Wang, Y. Wu, S. Zhao and Z. Wang, *Chem. Eng. J.*, **380**, 122600 (2020).
22. Z. Sun, H. Wang, Z. Wu and L. Wang, *Catal. Today*, **300**, 160 (2018).
23. X. Chen, Y. Li and L. Li, *Appl. Surf. Sci.*, **508**, 1 (2020).
24. X. Chen, W. Zhang, L. Zhang, L. Feng, J. Wen, J. Yang, C. Zhang, J. Jiang and H. Wang, *Appl. Surf. Sci.*, **481**, 1335 (2019).
25. Z. Ezzeddine, I. Batonneau-Gener, Y. Pouilloux and H. Hamad, *J. Mol. Liq.*, **223**, 763 (2016).
26. P. M. K. Reddy, P. Verma and C. Subrahmanyam, *J. Taiwan Inst. Chem. Eng.*, **58**, 500 (2016).
27. T. Wang, X. Liu, C. Ma, Y. Liu, H. Dong, W. Ma, Z. Liu, M. Wei, C. Li and Y. Yan, *J. Taiwan Inst. Chem. Eng.*, **93**, 298 (2018).
28. S. Megala, M. Sathish, S. Harish, M. Navaneethan, S. Sohila, B. Liang and R. Ramesh, *Appl. Surf. Sci.*, **509** 144656 (2020).
29. S. Tonda, S. Kumar, M. Bhardwaj, P. Yadav and S. Ogale, *ACS Appl. Mater. Interfaces*, **10**, 2667 (2018).
30. S. Nayak, L. Mohapatra and K. Parida, *J. Mater. Chem. A*, **3**, 18622 (2015).
31. T. Li, G. H. Li, L. H. Li, L. Liu, Y. Xu, H. Y. Ding and T. Zhang,

ACS Appl. Mater. Interfaces, **8**, 2562 (2016).
32. H. Hu, J. Liu, Z. Xu, L. Zhang, B. Cheng and W. Ho, *Appl. Surf. Sci.*, **478**, 981 (2019).
33. S. Xia, F. Liu, Z. Ni, J. Xue and P. Qian, *J. Colloid Interface Sci.*, **405**, 195 (2013).
34. Z. Peng, Y. Xin, X. Dong and Z. Quan, *Ceram. Int.*, **40**, 2115 (2014).
35. Y. Ao, D. Wang, P. Wang, C. Wang, J. Hou and J. Qian, *Mater. Res. Bull.*, **80**, 23 (2016).
36. P. Wang, D. H. L. Ng, M. Zhou and J. Li, *Appl. Clay Sci.*, **178**, 105131 (2019).
37. B. N. Mahato, T. Krithiga and M. A. M. Thangam, *Surf. Interfaces*, **23**, 100636 (2021).
38. H. Ouassif, E. M. Moujahid, R. Lahkale, R. Sadik, F. Z. Bouragba, E. m. Sabbar and M. Diouri, *Surf. Interfaces*, **18**, 100401 (2020).
39. L. Lu, J. Li, D. H. L. Ng, P. Yang, P. Song and M. Zuo, *J. Ind. Eng. Chem.*, **46**, 315 (2017).
40. I. Langmuir, *J. Am. Chem. Soc.*, **40**, 1361 (1918).
41. S. Chilukoti and T. Thangavel, *Inorg. Chem. Commun.*, **100**, 107 (2019).
42. B. Li, Y. Zhang, X. Zhou, Z. Liu, Q. Liu and X. Li, *J. Alloys Compd.*, **673**, 265 (2016).
43. Y. Zhou, J. Li, Y. Yang, B. Luo, X. Zhang, E. Fong, W. Chu and K. Huang, *J. Alloys Compd.*, **788**, 1029 (2019).
44. S. Li, Y. Yang, S. Huang, Z. He, C. Li, D. Li, B. Ke, C. Lai and Q. Peng, *Appl. Clay Sci.*, **188**, 105414 (2020).
45. K. V. Kumar and K. Porkodi, *Chem. Eng. J.*, **148**, 20 (2009).
46. S. A. A. Moaty, A. A. Farghali, M. Moussa and R. Khaled, *J. Taiwan Inst. Chem. Eng.*, **71**, 441 (2017).
47. Z. Zhou, S. Ouyang, P. Li, L. Shan, R. Ma and P. Zhang, *Appl. Clay Sci.*, **188**, 105500 (2020).
48. P. Sirajudheen, P. Karthikeyan, K. Ramkumar and S. Meenakshi, *J. Mol. Liq.*, **318**, 114200 (2020).

Supporting Information

Impact of g-C_3N_4 loading on NiCo LDH for adsorptive removal of anionic and cationic organic pollutants from aqueous solution

Harpreet Kaur, Satnam Singh, and Bonamali Pal[†]

School of Chemistry and Bio-Chemistry, Thapar Institute of Engineering and Technology, Patiala, 147004, India
(*Received 15 December 2020 • Revised 24 February 2021 • Accepted 13 March 2021*)

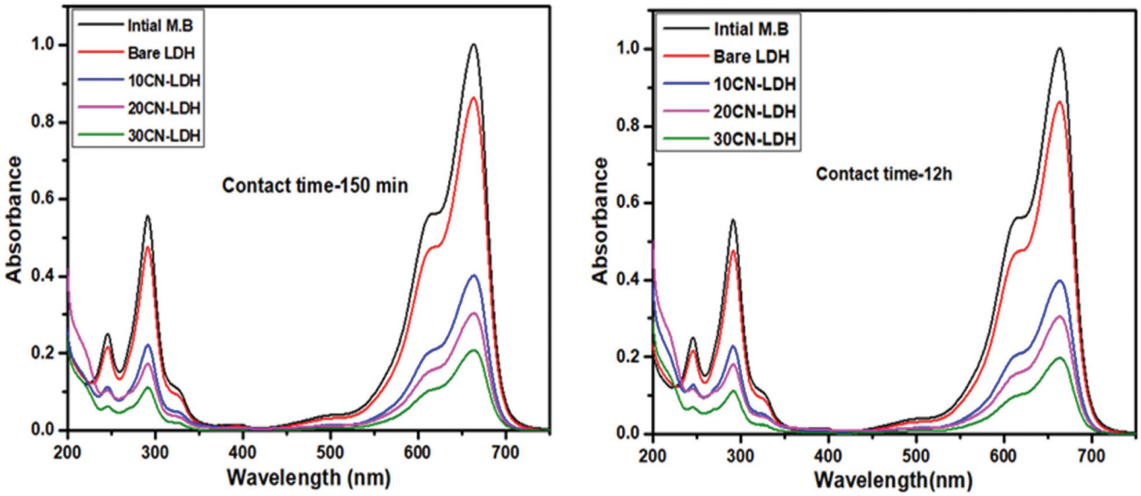

Fig. S1. Absorbance spectra of adsorption of methylene blue over bare LDH and (10-30) CN-LDH composites in 150 min (left) and 12 hours (right).

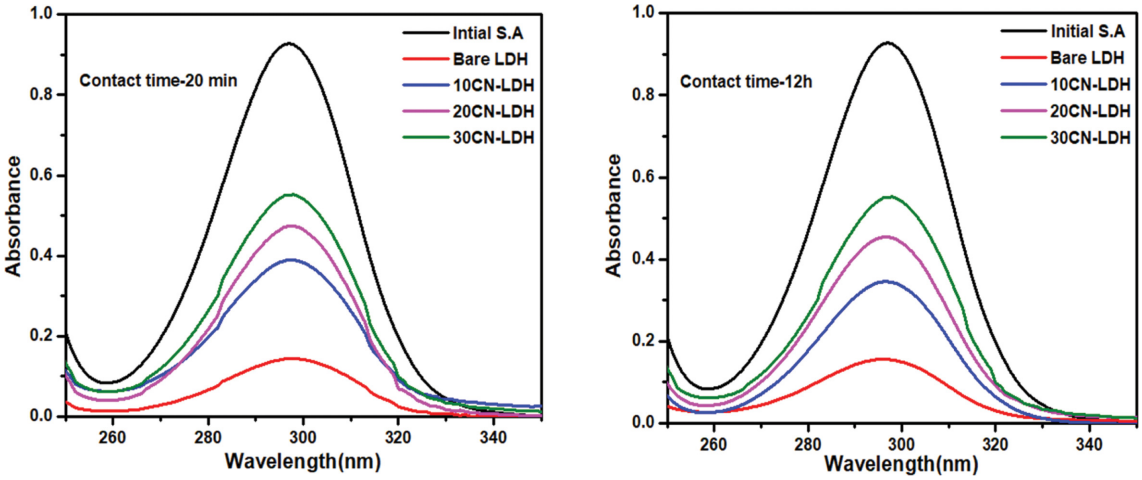

Fig. S2. Absorbance spectra of adsorption of salicylic acid over bare LDH and (10-30) CN-LDH composites in 20 min (left) and 12 hours (right).

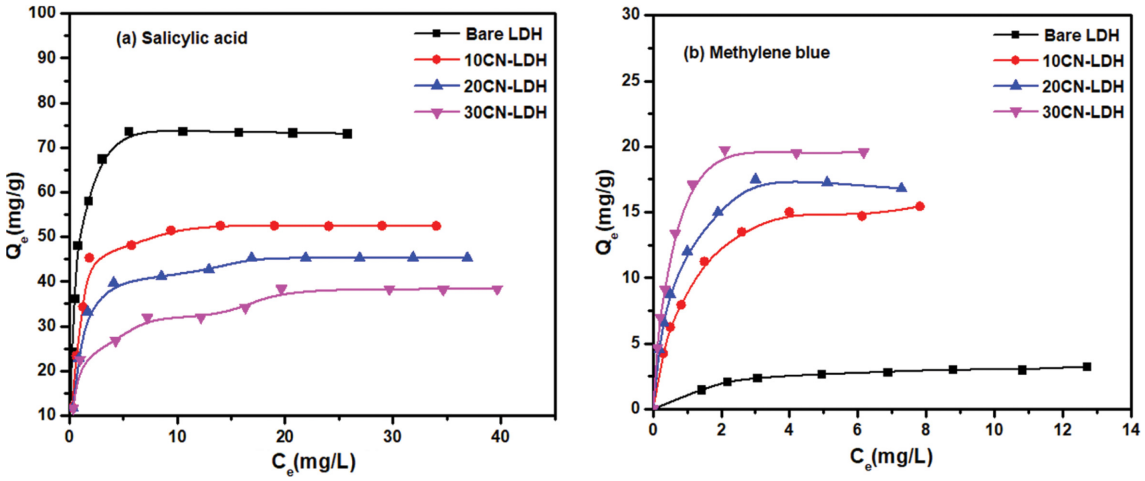

Fig. S3. Adsorption of salicylic and methylene blue over bare LDH and (10-30) CN-LDH composites.

Table S1. The analysis of zeta potential of bare LDH and (10-30) CN-LDH composites after the adsorption of salicylic acid and methylene blue

Adsorbent	Initial zeta potential (mV)	Zeta potential after salicylic acid adsorption (mV)	Zeta potential after methylene blue adsorption (mV)
Bare LDH	+27.7	−0.41	+29.7
10CN-LDH	+10.6	−1.21	+12.3
20CN-LDH	+6.69	−2.94	+9.98
30CN-LDH	+3.36	−4.82	+8.46